Femtosecond Laser Irradiation of Fused Silica with a Nanometric Inhomogeneity

Anton Rudenko, **Jean-Philippe Colombier**, **and Tatiana E. Itina**
Laboratoire Hubert Curien, UMR CNRS 5516, Lyon University
Bât F, 18 rue du Prof. Benoît Lauras, Saint-Etienne 42000, France

Abstract— A finite-difference time-domain (FDTD) method based on Maxwell's equations coupled with time-dependent electron carrier density equation is proposed to investigate numerically femtosecond laser irradiation of dielectrics with a small inhomogeneity. The process of plasma generation due to multiphoton absorption near small defect in fused silica is studied in details and local field distribution around the inhomogeneity is first explained by using the Rayleigh scattering theory. Further investigation of the laser-matter interaction shows that the generated plasma properties do not significantly depend on the size of the inhomogeneity as long as it remains considerably smaller than the irradiation wavelength. The calculation results show, however, that there are several parameters which are crucial. Among such parameters, for instance, is the collision frequency, which affects strongly both the created electron density and laser propagation. In addition, the changes in the refractive index of the plasma are taken into account by the Lorentz-Drude model with time-dependent carrier density. The differences between the results calculated by using Keldysh theory for multiphoton ionization and obtained by considering only six-photon ionization are discussed. Finally, temporal changes in the behavior of scattering due to generated nanoplasma are observed and analyzed by using Mie scattering theory, which is more complete than Rayleigh one.

1. INTRODUCTION

Over past decades significant progress has been achieved in the field offemtosecond laser interaction with dielectric materials, in particular,with the possibility to induce different kind of modifications in transparent materials. Ultra-short laser beams achieve periodic nanostructuring, characterized by a sub-wavelength period [1]. These self-organized structures emerge spontaneously during multi-pulse irradiation and the conditions triggering their formation remain poorly explored. Small defects in dielectrics reinforce damage during femtosecond laser irradiation and lead to the generation of nanoplasmas, thus affecting laser propagation. Local refractive index changes in the media due to this damage lead to other nonlocal physical phenomena, as, for instance,strong interference of the incident wave with the plasma wave [1] incubation processes in plasma [2, 3] thermal diffusion or self-trapping of excitons [4, 6], thus resulting into a feedback for nanograting formation.

The nature, the size and the shape of the initial defects were found to significantly vary and potentially play an important role in the nanograting initiation. However, the processes of plasma generation after the first pulse irradiation for small impurity center typically leads to the formation of the larger defects due to the memory in nonlinear ionization of transparent solids [5]. In this article we consider inhomogeneities with different properties, by varying its size in the nanometric scale. Sphere is chosen as the simplest shape, for which there are analytical solutions of the Mie scattering problem [7]. Herein it is supposed that initial defects have nanometric scale and are smaller than the wavelength of the irradiation. FDTD method [8], based on Maxwell's equations coupled with time-dependent electron carrier density equation is applied to investigate numerically femtosecond laser irradiation of dielectrics with inhomogeneities, where nonlinear effects of multiphoton ionization and Kerr non-linearity are included.

2. SIMULATION MODEL

To better understand the processes of laser interaction with small inhomogeneities in dielectrics, the finite-difference time-domain (FDTD) approach for nonlinear and disperse media is applied [8]. In this method Maxwell's equations are written as:

$$\begin{cases} \frac{\partial}{\partial t}\overrightarrow{D} = \nabla \times \overrightarrow{H} - \overrightarrow{J} \\ \frac{\partial}{\partial t}\overrightarrow{H} = -\frac{\nabla \times \overrightarrow{E}}{\mu_0} \end{cases} \quad (1)$$

where $\overrightarrow{D}$ is the displacement field, $\overrightarrow{E}$ is the electric field, $\overrightarrow{H}$ is the magnetic field and $\overrightarrow{J}$ is the current density. They are numerically solved by using the standard Yee's algorithm [8]. At the edges of the grid absorbing boundary conditions related to convolutional perfect matched layers (CPML) are set to avoid nonphysical reflections [9]. Substitution of the constitutive equations into Maxwell-Ampere equation yields:

$$\frac{\partial}{\partial t}\vec{E} = \frac{\nabla\times\vec{H}}{\varepsilon_0} - \frac{1}{\varepsilon_0}\left(\vec{J}_{L-D} + \vec{J}_{\mathrm{Kerr}} + \vec{J}_{\mathrm{MPI}}\right), \tag{2}$$

where $\vec{J}_{L-D}$ is current derived from the Lorentz-Drude model for the dispersive media; $\vec{J}_{\mathrm{Kerr}}$ is Kerr polarization current; and $\vec{J}_{\mathrm{MPI}}$ is the multiphoton ionization term. For dielectric materials, such as fused silica, the heating of the conduction band electrons is modeled by Drude model with time-dependent carrier density as follows:

$$\frac{\partial}{\partial t}\vec{J_D} = -\nu_e\vec{J_D} + \frac{e^2 n_e}{m_e}\vec{E} \tag{3}$$

where e is the elementary charge; m_e is the mass of an electron; n_e is the carrier electron density and ν_e is the electron collision frequency. For metals, as gold or silver, Lorentz-Drude model is applied.

$$\frac{\partial^2\vec{J_m}}{\partial t^2} + \gamma_m\frac{\partial\vec{J_m}}{\partial t} + \omega_m^2\vec{J_m} = G_m\omega_p^2\frac{\partial\vec{E}}{\partial t} \tag{4}$$

where $\gamma_m\omega_m$ and G_m are the damping factor, resonance frequency and oscillator strength respectively for each Lorentz pole m, and $\omega_p = \frac{e^2 n_e}{m_e}$ is the plasma frequency, and $\vec{J_L} = \sum_m \vec{J_m}$ is the resulting current for dispersive medium.

In addition, nonlinearity of the third order is included, which describes Kerr effect, as follows:

$$\vec{J}_{\mathrm{Kerr}} = \varepsilon_0\chi_3\frac{\partial\left(\left|\vec{E}\right|^2\vec{E}\right)}{\partial t} \tag{5}$$

where the third-order susceptibility is $\chi_3 = 2\cdot 10^{-22}\,\mathrm{m}^2V^{-2}$ [10].

For multiphoton ionization, two approaches are used and compared: the complete Keldysh theoretical equation [11], including multiphoton and tunneling ionization, for which the corresponding current can be written as:

$$\vec{J}_{\mathrm{MPI}} = E_g\frac{w_{\mathrm{Keldysh}}\vec{E}}{I}\frac{n_a - n_e}{n_e} \tag{6}$$

and a simplified six-photon ionization model, which is as an approximation at low laser intensities for an excitation wavelength of $\lambda = 800\,\mathrm{nm}$, as

$$\vec{J}_{\mathrm{MPI}} = E_g\sigma_6 I^5\vec{E}\frac{n_a - n_e}{n_e} \tag{7}$$

Here $E_g = 9\,\mathrm{eV}$ is the electron band gap in the absence of the electric field; $n_a = 2\cdot 10^{28}\,\mathrm{m}^{-3}$ is the saturation density; $I = \frac{n}{2}\sqrt{\frac{\varepsilon_0}{\mu_0}}|\vec{E}|^2$ — intensity; $n = 1.45$ is the refractive index of unexcited fused silica for $\lambda = 800\,\mathrm{nm}$. Keldysh ionization rate (w_{Keldysh}) and the six-photon ionization rate ($\sigma_6 I^6$) for $\sigma_6 = 2\cdot 10^{-65}\,\mathrm{m}^9\mathrm{W}^{-6}\mathrm{s}^{-1}$ [9] and $\sigma_6 = 2\cdot 10^{-67}\,\mathrm{m}^9\mathrm{W}^{-6}\mathrm{s}^{-1}$) [12] are compared. As the intensities reached in our simulations are from $I = 10^{16}$ to $10^{18}\,\mathrm{W/m}^2$ and are above the ablation threshold, it is also important to take into account the tunneling ionization effect and consider the complete Keldysh ionization rate. Moreover, applying six-photon ionization model [10] typically considered as a good approximation for low intensities, leads to the overestimation of ionization rate by up to three orders of magnitude in our intensity interval. On the contrary, another approximated model [12] gives underestimated values for the ablation threshold. Therefore, the complete Keldysh expression is proven to be the most appropriate one for photoionization in our case.

Then, Maxwell's equations are coupled with the rate equation for free carrier number density as follows

$$\frac{\partial n_e}{\partial t} = W_{\mathrm{MPI}} + W_{av} - \frac{n_e}{\tau_{tr}} \tag{8}$$

where the first term on the left corresponds to the multiphoton ionization

$$W_{\text{MPI}} = (n_a - n_e) w_{\text{Keldysh}} \tag{9}$$

and $\tau_{tr} = 150\,\text{fs}$ is the electron trapping time [10].

The system of nonlinear equations is resolved by the fixed-point iteration algorithm similar to the iteration algorithms developed in [13, 14].

Here, the initial Gaussian electric field profile is considered as a focused beam source taking the following form:

$$E_x(t,x,y,z) = E_0 \frac{w_0}{w(z)} \exp(-\frac{r^2}{w(z)^2} - ikz - ik\frac{r^2}{2R(z)} + i\varsigma(z)) e^{-2\ln 2\left(\frac{t-t_0}{\theta}\right)^2} e^{i\omega t} \tag{10}$$

where $r^2 = x^2 + y^2 + z^2$ is the radial distance from the center axis of the beam, $w_0 = 1.5\,\mu\text{m}$ is the beam waist, $w(z) = w_0\sqrt{1 + (\frac{z}{z_R})^2}$ is the spot size; $R(z) = z[1 + (\frac{z_R}{z})^2]$ is the radius of curvature, $z_R = \frac{\pi w_0^2 n_0}{\lambda}$ is the Rayleigh length; $\varsigma(z) = \arctan(\frac{z}{z_R})$ is the Gouy phase shift; $\theta = 70\,\text{fs}$ is the pulse width at half maximum (FWHM); and $t_0 = 125\,\text{fs}$ is a time delay. For the given waist beam and irradiation wavelength of $\lambda = 800\,\text{nm}$, the numerical aperture is $\text{NA} = n\sin(\frac{\lambda}{\pi w_0}) \approx 0.169$. Note that for this aperture the paraxial approximation of the Gaussian beam profile is still valid [15, 16].

3. RESULTS AND DISCUSSION

To better understand the process of the first femtosecond laser pulse interaction with the material in the presence of a localized defect, we consider firstly its interaction with a small spherical metallic nanoparticle. For this, it is convenient here to define two dimensionless parameters, a size parameter $q = 2\pi a/\lambda_1$, where a is radius of sphere defect, λ_1 is laser wavelength in the dielectric media; and $n^2 = \varepsilon_2/\varepsilon_1$ is a relative permeability, where ε_1, ε_2 are permeabilities of the media and of the inhomogeneity, respectively. The local field distribution strongly depends on these parameters according to the Mie theory.

In the present study, we consider, that the conditions $q \ll 1$ and $nq \ll 1$ are satisfied, so that the scattering has a dipole character. For instance, for nanoparticles with radius $a \ll 90\,\text{nm}$ the condition is valid at laser irradiation wavelength $\lambda_1 \approx 550\,\text{nm}$ in fused silica. In this case, the approximation of the scattered electric field can be derived from the general analytical solution of Maxwell's equations for an electromagnetic plane wave, scattered by the homogeneous sphere, or Mie scattering [7], under the discussed conditions assuming that the first electric dipole moment ${}^eB_1$ is higher than all magnetic ${}^mB_n$ and the other electric ones [17]. However, when the relative permeability is high (metallic case), the Rayleigh approximation (condition $nq \ll 1$) is no more applied and magnetic dipole moments should be also considered.

In the near-field approximation ($kr \ll 1$, r is radial distance from the center of the nanoparticle), scattered electric fields can be written in the following form [17]:

$$\begin{aligned} E_r^{(s)} &= -\frac{2i\cos\varphi\sin\theta}{(kr)^3}{}^eB_1 \\ E_\theta^{(s)} &= \frac{\cos\varphi}{kr}\left\{\frac{i\cos\theta^e B_1}{(kr)^2} + \frac{{}^mB_1}{kr}\right\} \\ E_\varphi^{(s)} &= -\frac{\sin\varphi}{kr}\left\{\frac{i^e B_1}{(kr)^2} + \frac{{}^mB_1\cos\theta}{kr}\right\} \end{aligned} \tag{11}$$

In what follows, we consider the polarization along x direction and light propagation along z direction. This way, both electric field $\overrightarrow{E}$ and wave vector $\overrightarrow{k}$ lie in xz plane (corresponding to $\varphi = 0$) and we consider the near-field laser-matter interaction in this plane. The intensity distribution can be estimated as (neglecting the magnetic dipole moments):

$$I^2 = E_\theta^{(s)}\overline{E_\theta^{(s)}} + E_r^{(s)}\overline{E_r^{(s)}} \approx \frac{(4\sin^2\theta + \cos^2\theta)({}^eB_1)^2}{(kr)^6} \tag{12}$$

From this expression,one can see that the intensity is higher in the x direction ($\theta = \pi/2$) than in the z direction ($\theta = 0, \pi$), creating elliptical distribution of intensities in the near-field of nanoparticle.

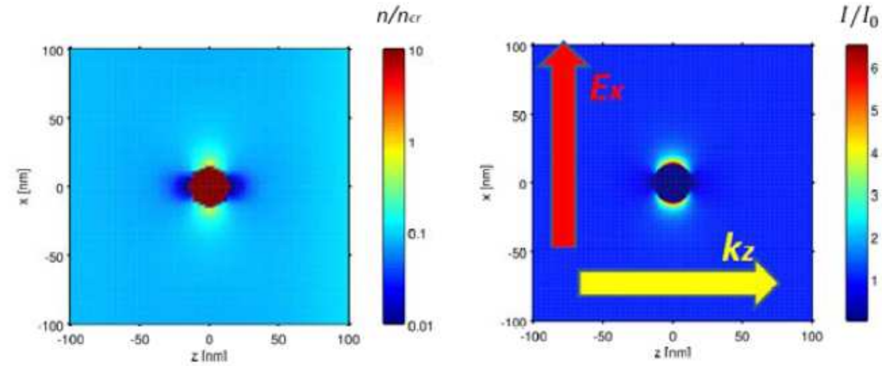

(a) (b)

Figure 1: Near-field approximation of the intensity distribution created by small gold nanoparticle given by (b) the analytical Mie solution and electron density distribution of fused silica generated plasma, calculated by using Equations (1)–(8), normalized to critical value $n_{cr} = 1.7 \cdot 10^{27}\,\mathrm{m}^{-3}$ at $\lambda = 800\,\mathrm{nm}$ irradiation near gold nanoparticle with parameter size $q = 0.2$ at the end of (a) the pulse. The input pulse has the energy of 250 nJ.

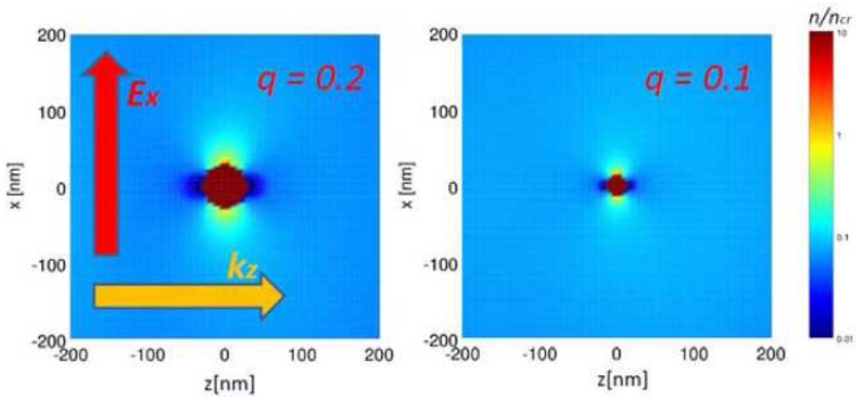

Figure 2: Electron density distributions of generated plasma, calculated by using Equations (1)–(8), normalized to critical value $n_{cr} = 1.7 \cdot 10^{27}\,\mathrm{m}^{-3}$ at $\lambda = 800\,\mathrm{nm}$ irradiation near gold nanoparticles of different size ($q = 0.2$ and $q = 0.1$) at the end of the pulse The input pulse has the energy of 250 nJ.

As the intensity increases and reaches the ablation threshold, the ionization processes start to play essential role and lead to the generation of plasma in the enhanced intensity regions. First hot spots will appear at the interface between fused silica and gold. An asymptotic solution of the Mie scattering problem for near-field of a small nanoparticle is presented in Fig. 1. The calculation results show that density distribution strictly follows the intensity one. The process of the plasma generation is quite similar for an inhomogeneity of a smaller size (Fig. 2), which gives us the opportunity to understand what happens in the near-field of very small defects considering nanoparticles larger in size. Assuming that after the first pulse, plasma has reached the critical density value $n_{cr} = 1.7 \cdot 10^{27}\,\mathrm{m}^{-3}$, we note that the new inhomogeneity will have metallic properties and can be considered as larger defect elongated in the polarization direction.

The process of plasma generation does not strongly depend on the size and on the exact nature of the defect. However the optical parameters of the media are crucial in the electromagnetic modeling. As frequency dependence of fused silica is described by Drude formalism, the complex permeability of the media, dependent also on the electronic carrier density, can be written in the following way:

$$\varepsilon(n_e) = \varepsilon_\infty - \frac{e^2 n_e}{m_e\left(\omega^2 + \nu_e^2\right)} + i\frac{e^2 n_e \nu_e}{m_e \omega\left(\omega^2 + \nu_e^2\right)} \tag{13}$$

where $\omega = \frac{2\pi c}{\lambda}$ is the frequency of the irradiated wavelength and ν_e is the electron collision frequency. In several works, the electron collision time, which in reality depends both on the electron carrier density and on the electron temperature, is assumed to be constant. The values commonly used

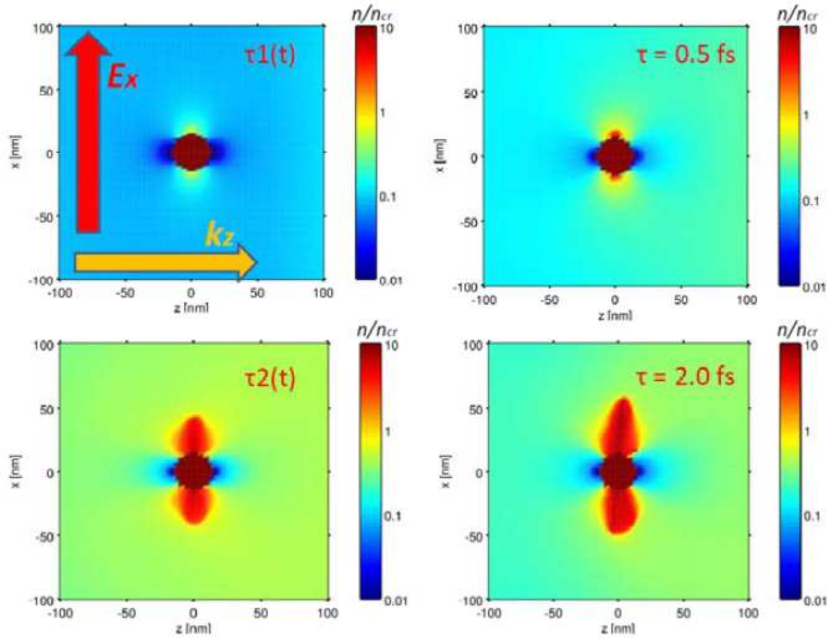

Figure 3: Electron density distributions, calculated by using Equations (1)–(8), normalized to fused silica critical value $n_{cr} = 1.7 \cdot 10^{27}\,\mathrm{m}^{-3}$ at $\lambda = 800\,\mathrm{nm}$ irradiation near gold nanoparticle for four different electron collision times models: $\tau 1(t)$, according to (14) used in Reference [19, 21]; $\tau = 0.5\,\mathrm{fs}$; $\tau 2(t)$, according to (15); and $\tau = 2.0\,\mathrm{fs}$. The input pulse has the energy of 300 nJ.

in the analysis of experimental measurements and in numerical simulations vary from 0.1 fs to 10 fs [18–22].

In this work, the calculations are first performed with $\tau = 1/\nu_e = 0.5\,\mathrm{fs}$. In addition, we take into consideration time-varying density-dependent electron collision time by using two different equations. One possibility is to use the following expression that was proposed in Drude models [20, 22]:

$$\begin{cases} \tau(t) = 3.5\,\mathrm{fs}, \quad n_e(t) \leq 5 \cdot 10^{25}\,\mathrm{m}^{-3} \\ \tau(t) = \frac{16\pi\varepsilon_0^2\sqrt{m_e^*(0.1E_g)^3}}{\sqrt{2}e^4 n_e(t)}, \quad n_e(t) \geq 5 \cdot 10^{25}\,\mathrm{m}^{-3} \end{cases} \tag{14}$$

where $E_g = 9\,\mathrm{eV}$ is the electron band gap and $m_e^* = 0.64 m_e$ — reduced electron mass. In the work [19] the comparison between the calculated reflectivity for different electron collision times and the experimental results obtained in [10] has been done.This comparison gives us the maxima and minima of the parameter which can be used in simulations.

In dielectric materials electron collision time also depends on electron mobility, so that the following empirical equation is to be checked out:

$$\tau_e(t) = \tau_{\min} + \frac{\tau_{\max} - \tau_{\min}}{1 + (n_e(t)/n_{cr})^{\alpha}}, \tag{15}$$

where $\tau_{\min} = 0.2\,\mathrm{fs}$; $\tau_{\max} = 2\,\mathrm{fs}$; and $\alpha = 0.7$. Thus, with growing density we obtain smaller values for collision time, which fits well the experimental results [10, 22, 23].

The calculation results obtained by using different parameters (constant electron collision times $\tau = 0.5\,\mathrm{fs}$ and $\tau = 2\,\mathrm{fs}$ and empirical relationships (14) and (15)) are shown in Fig. 3. One can see that the results obtained by using Equation (14) are closer to the ones obtained for $\tau = 0.5\,\mathrm{fs}$ and reveal smaller effects of the particles, whereas the results calculated by using Equation (15) are closer to the case with $\tau = 2\,\mathrm{fs}$ and demonstrate stronger changes in the field around the particle. One can notice a slight asymmetry in the density distribution in "x" direction relative to the collision time of 2 fs in Fig. 3. This asymmetry comes from the numerical scheme which should be improved, the work is underway.

In what follows, we compare the density distributions of the fused silica plasma generated in the near-field of the gold nanoparticle after the end of the pulse. The higher the collision time is,

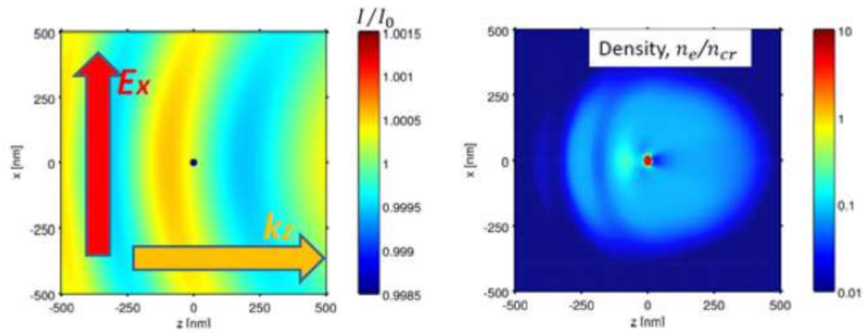

Figure 4: Far-field resulted intensity distribution (interference with plane wave) for a small gold nanoparticle and electron density distribution image of a Gaussian beam tightly focused in fused silica with a small inhomogeneity showing how the light propagation might be further affected and new plasma generated in the maxima of the resulted intensity. Electron density, calculated by using Equations (1)–(8), is normalized to fused silica critical value $n_{cr} = 1.7 \cdot 10^{27}\,\mathrm{m}^{-3}$ at $\lambda = 800\,\mathrm{nm}$ irradiation. The input pulse has the energy of 250 nJ.

the closer the properties of the media to the metallic ones. Moreover, the one can note, that the electron collision time which corresponds to the near-critical density value plays a crucial role in plasma generation. Thus, in the first proposed empirical model (14) $\tau_1(n_{cr}) \approx 0.1\,\mathrm{fs}$ and in the (15) $\tau_2(n_{cr}) \approx 1.1\,\mathrm{fs}$. These facts explain the differences in the calculation results.

Finally we investigate how the generated plasma near small defect affects the laser propagation. We start from the far-field approximation ($kr \gg 1$) [17]:

$$\begin{aligned} E_r^{(s)} &= -\frac{2\cos\varphi\sin\theta}{k^2r^2}\,{}^eB_1\exp(ikr) \\ E_\theta^{(s)} &= -\frac{i\cos\varphi}{kr}\exp(ikr)\left\{{}^eB_1\cos\theta + {}^mB_1\right\} \\ E_\varphi^{(s)} &= \frac{i\sin\varphi}{kr}\exp(ikr)\left\{{}^eB_1 + {}^mB_1\cos\theta\right\} \end{aligned} \tag{16}$$

Due to the interference of the incident wave with the scattered spherical wave, the periodic maxima and minima will be organized and they will lead to the regions of the enhanced density. However, the intensity decreases very fast in the radial direction, as $1/r^2$, explaining why local maxima are getting weaker. We consider, as for the near-field problem, the laser interaction with the defect in xz plane, corresponding to $\varphi = 0$. Note, in this case $E_\varphi^{(s)} = 0$ and in the far-field $E_\theta^{(s)} \gg E_r^{(s)}$. Converting the scattered electric field to Cartesian coordinates, we see that there is a scattered component $E_x^{(s)} \sim \frac{\exp(ikz)}{kz}$ which interferes with the incident wave $E_x^{(i)} \sim \exp(-ikz)$ and this interference leads to maxima and minima in the axis z backward direction. The interference diagram between asymptotic for the Mie scattering problem, a solution in the far-field for a small inhomogeneity and a plane wave are shown in Fig. 4. The density distribution calculated by FDTD is also presented in the figure, where the interference leads to the organization of the second nanoplasma structure created in backward direction of laser propagation.

4. CONCLUSION

We have investigated numerically nanoplasma formation near different kind of defects due to tight focusing during femtosecond laser irradiation. It is shown that the transient properties of the material surrounding the defect object strongly impact the distribution and the size of the generated plasma. Therefore, collisional frequency is the parameter which is crucial for electromagnetic modeling. The size of inhomogeneity and its associated electron number density (if they satisfy Rayleigh approximations $q \ll 1$ and $nq \ll 1$) are less important. Each considered inhomogeneity leads to the generation of the plasma in the near-field of the impurity center and spreading of the defect zone in form of ellipsoid. As the inhomogeneity grows, the scattering wave from it interacts with the incident wave. As a result of the interference in the far-field the density maxima are found to appear and new plasma regions are generated. These results demonstrate how the small defects can evaluate and how the light interaction is further affected due to their formation during the femtosecond laser irradiation.

ACKNOWLEDGMENT

This work was supported by the LABEX MANUTECHSISE (ANR-10-LABX-0075) of Université de Lyon, within the program "Investissements d'Avenir" (ANER-11-IDEX-0007) operated by the French National Research Agency (ANR).

REFERENCES

1. Shimotsuma, Y., et al., "Self-organized nanogratings in glass irradiated by ultrashort laser pulses," *Phys. Rev. Lett.*, Vol. 91, No. 24, 2003.
2. Liang, F., et al., "Role of ablation and incubation processes on surface nanograting formation," *Optical Materials Express*, Vol. 1, No. 7, 2011.
3. Buschlinger, R., S. Nolte, and U. Peschel, "Self-organized pattern formation in laser-induced multiphoton ionization," *Ph. Rev. B*, Vol. 89, 184306, 2014.
4. Richter, S., et al., "The role of self-trapped excitons and defects in the formation of nanogratings in fused silica," *Optics Letters*, Vol. 37, No. 4, 2012.
5. Rajeev, P., et al., "Memory in nonlinear ionization of transparent solids," *Phys. Rev. Lett.*, Vol. 97, 253001, 2006.
6. Martin, P., S. Guizard, et al., "Subpicosecond study of carrier trapping dynamics in wide-band-gap crystals," *Phys. Rev. B*, Vol. 55, No. 9, 1997.
7. Mie, G., *Ann. Phys.*, Vol. 25, 377, 1908.
8. Yee, K. S., "Numerical solution of initial boundary value problems involving Maxwell's equations in isotropic media," *IEEE Trans. on Antennas and Propagat.*, Vol. 14, No. 3, 302–307, 1966.
9. Roden, J. A. and S. D. Gedney, "Convolution PML (CPML): An efficient FDTD implementation of the CFS-PML for arbitrary media," *Microwave and Optical Technology Letters*, Vol. 27, No. 5, 334–339, 2000.
10. Gamaly, E., "Laser-matter interaction in the bulk of a transparent solid: Confined microexplosion and void formation," *Phys. Rev. B*, Vol. 73, 214101, 2006.
11. Keldysh, L. V., "Ionization in the field of a strong electromagnetic wave," *Soviet. Phys. JETP*, Vol. 20, No. 5, 1307–1314, 1965.
12. Couairon, A., "Filamentation and damage in fused silica induced by tightly focused femtosecond laser pulses," *Phys. Rev. B*, Vol. 71, 125435, 2005.
13. Greene, J. and A. Taflove, "General vector auxiliary differential equation finite-difference time-domain method for nonlinear optics," *Optics Express*, Vol. 14, No. 18, 2006.
14. Ammann, M., "Non-trivial materials in EM-FDTD," Master's Thesis, Department of Physics, Swiss Federal Institute of Technology, 2007.
15. Bulgakova, N. M., V. P. Zhukov, and Y. P. Meshcheryakov, "Theoretical treatments of ultrashort pulse lasers processing of transparent materials: Toward understanding the volume nanograting formation and "quill" writing effect," *Appl. Phys. B*, Vol. 113, 437–449, 2013.
16. Bulgakova, N. M., V. P. Zhukov, et al., "Pulsed laser modification of transparent dielectrics: What can be foreseen and predicted in numerical experiments?," *J. Opt. Soc. Am. B*, Vol. 31, No. 11, 2014.
17. Born, M. and E. Wolf, *Principles of Optics*, 4th Edition, Pergamon Press, 1970.
18. Sudrie, L., et al., "Femtosecond laser-induced damage and filamentary propagation in fused silica," *Phys. Rev. Lett.*, Vol. 89, No. 18, 2002.
19. Varkentina, N., O. Uteza, N. Sanner, B. Chimier, M. Sentis, and T. Itina, "Absorption of femtosecond laser pulse in fused silica: Experiments and modelling," *Proc. of SPIE*, Vol. 7920, 792003-1, 2011.
20. Jing, X., et al., "Modeling validity of femtosecond laser breakdown in wide bandgap dielectrics," *Appl. Surf. Sci.*, Vol. 258, 4741–4749, 2012.
21. Gamaly, E. and A. Rode, "Transient optical properties of dielectrics and semiconductors excited by an ultrashort laser pulse," *J. Opt. Soc. Am. B*, Vol. 31, No. 11, 2014.
22. Starke, K., et al., "Investigations in the non-linear behavior of dielectrics by using ultrashort pulses," *Proc. of SPIE*, Vol. 5273, 501–514, 2004.
23. Sun, Q., et al., "Measurement of the collision time of dense electronic plasma induced by a femtosecond laser in fused silica," *Optics Letters*, Vol. 30, No. 3, 2005.